Production and Purification of Anhydrous Sodium Sulfide

Journal:	*Journal of Sulfur Chemistry*
Manuscript ID	GSRP-2020-0176.R1
Manuscript Type:	Research Article
Date Submitted by the Author:	n/a
Complete List of Authors:	Smith, William; Colorado School of Mines, Chemical & Biological Engineering Birnbaum, Jerry; Colorado School of Mines, Chemical & Biological Engineering Wolden, Colin; Colorado School of Mines, Chemical & Biological Engineering
Keywords:	reagent, sodium sulfide, anhydrous, Hydrogen sulfide, battery

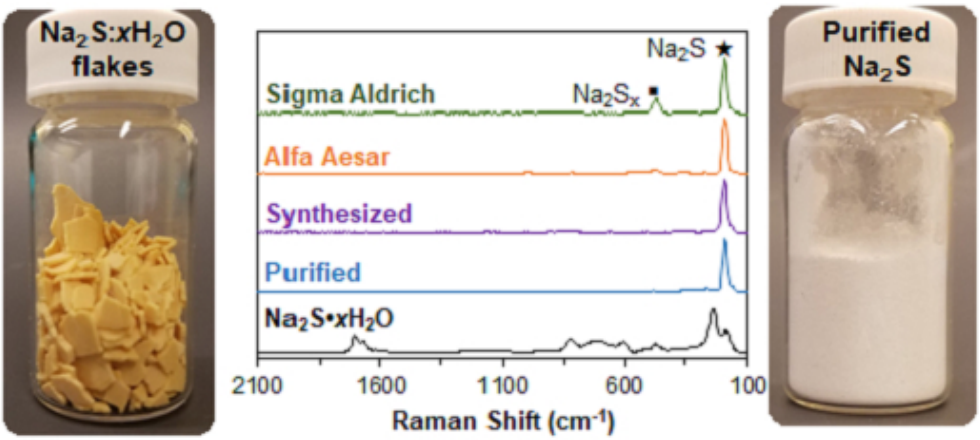

138x61mm (96 x 96 DPI)

Production and Purification of Anhydrous Sodium Sulfide

William H. Smith,[a] Jerry Birnbaum,[a] and Colin A. Wolden[a]*

[a]*Chemical and Biological Engineering, Colorado School of Mines, Golden, CO, USA;*

*Corresponding author email: cwolden@mines.edu

Production and Purification of Anhydrous Sodium Sulfide

ABSTRACT: Anhydrous sodium sulfide (Na_2S) is a key component in sodium-sulfur batteries as well as an important chemical reagent. However, anhydrous Na_2S is currently prohibitively expensive for applications outside of research labs and purity is a concern. Herein, we compare the properties of three forms of anhydrous Na_2S: (i) commercially supplied, (ii) Na_2S produced through dehydration and purification of commercial hydrate flakes ($Na_2S•xH_2O$), and (iii) Na_2S formed by the reaction of hydrogen sulfide with dissolved sodium alkoxide and recovered through solvent evaporation. Crystallinity, purity, thermal stability, and morphology of the various forms of Na_2S were characterized by XRD, FTIR/Raman, TGA, and SEM respectively. Vacuum annealing of low-cost Na_2S hydrate at 150 °C produced anhydrous Na_2S. This dehydrated material retains impurity signatures attributed to polysulfide (Na_2S_x) and oxysulfur impurities (SO_x) that were also observed in commercially supplied Na_2S. Impurity removal typically requires hydrogen reduction at very high temperature (700-900ºC), but it is demonstrated here that this can instead be accomplished at 400 ºC, preventing auto-oxidation and following kinetics well-described by a shrinking core model. The solution-based approach resulted in the direct synthesis of crystalline Na_2S anhydride at low temperatures (100 °C) without need for further purification. Both approaches presented herein are inherently scalable with materials costs that are one to two orders of magnitude lower than the current price of anhydrous Na_2S.

Keywords: sodium sulfide; sodium batteries; metal sulfides

1. Introduction

High-purity, anhydrous Na_2S is a key material for several applications including energy storage, chemical synthesis, and as an H_2S generator in biological systems. For example, Na_2S nanocrystals can serve in high-capacity cathodes for low-cost, high-energy-density Na-S batteries.[1-3] Na_2S is also a key precursor for solid state electrolytes that may enable the safe use of a sodium-metal anode.[4-6] Additionally, Na_2S is a convenient reagent for the synthesis of specialty chemicals ranging from sulfide-containing polymers to a broad selection of metal-

sulfide compounds.[7-10] Lastly, Na_2S has gained attention as a "rapid-release" donor of H_2S in aqueous solutions, which is a crucial gasotransmitter, with potential for several medical therapeutic applications ranging from cardiovascular to neurological diseases. The purity of Na_2S intended for therapeutic applications is crucial because polysulfide and oxysulfur impurities may cause unintended biological effects.[11] In contrast to the earth abundance of its constituent elements, anhydrous Na_2S is prohibitively expensive (>\$10 g^{-1}), an issue that must be addressed to enable widespread deployment of the technologies discussed above.

The high cost of anhydrous Na_2S reflects the difficulty to synthesize and purify this key material. Anhydrous Na_2S is produced primarily through two routes:[12]

(**1**) $$Na_2SO_4 + 2C \xrightarrow{\Delta} Na_2S + 2CO_2$$

(**2**) $$Na_2S{\bullet}9H_2O \xrightarrow{\Delta} Na_2S + 9H_2O$$

In the first route, Na_2SO_4 undergoes carbothermal reduction in a furnace at 900-1,000 °C, which is time- and energy-intensive, and directly emits carbon dioxide. The second route is preferred for applications where high purity is crucial and consists of three steps. First, Na_2S is dissolved in water to form a supersaturated solution. Second, $Na_2S{\bullet}9H_2O$ is recrystallized from the solution at relatively high purity (e.g. 98%). The recrystallization process is expensive and time-consuming, and results in a hydrate that only consists of 32 wt% Na_2S. Last, the nonahydrate is heated to elevated temperatures (> 700 ºC) to drive off water and induce crystallization. Therefore, there is a need for economically viable and inherently scalable methods of producing high-purity anhydrous Na_2S.

A low-grade form of Na_2S is also produced as a byproduct of several industrial processes, including caustic scrubbing of natural gas and processing of sulfide-containing ores like

BaS.[12] This "technical" grade of Na_2S is commercially available at low cost (~\$0.50 kg^{-1} in bulk quantities), but in the form of a hydrate ($Na_2S•xH_2O$, x~3) that contains ~40 wt% water. Its characteristic yellow color reflects the presence of polysulfide impurities (Na_2S_x). In addition to polysulfides, this Na_2S hydrate contains significant concentrations of oxysulfur impurities (Na_2SO_x) such as sodium sulfate, sulfite, thiosulfate, and hyposulfite. The hydrate also typically contains a high concentration of sodium hydrosulfide (NaHS). As such, this grade of Na_2S finds use in applications where purity and moisture content is not of concern, such as in the Kraft process in the pulping industry or as a bleaching agent in the manufacture of textiles or rubber. Efficient purification of this low-grade form of Na_2S would be an economically attractive route to anhydrous Na_2S for the applications listed above.

Alternatively, we have developed a solution-based approach based on green chemistry for the synthesis of alkali metal sulfide (Li_2S, Na_2S) nanocrystals (NCs).[13] Reactive precipitation of anhydrous sulfide NCs was achieved through a two-step process where an alkoxide precursor is first prepared by complexing the alkali metal with alcohol, which also liberates clean-burning hydrogen (**3**). In the second step the industrial waste hydrogen sulfide (H_2S) is bubbled through the solution resulting in NC precipitation and regeneration of the alcohol reagent (**4**). The net reaction (**5**) is the conversion of the alkali metal into a sulfide NC with co-generation of H_2 and full abatement of the H_2S. These spontaneous reactions proceed to completion with an atom economy approaching unity at ambient temperature and pressure.

(**3**) $$2M_{(s)} + 2ROH_{(sln)} \xrightarrow{RT,\ 1\ atm} 2ROM_{(sln)} + H_{2(g)}$$

(**4**) $$H_2S_{(g)} + 2ROM_{(sln)} \xrightarrow{RT,\ 1\ atm} M_2S_{(s)} + 2ROH_{(l)}$$

(**5**) $$2M_{(s)} + H_2S_{(g)} \xrightarrow{RT,\ 1\ atm} M_2S_{(s)} + H_{2(g)}$$

Both anhydrous Li_2S and Na_2S were successfully produced, and we developed a novel 4-phase bubble column for conducting reactive precipitation in a scalable fashion.[14] Precipitation is induced by the presence of a co-solvent, and NC size and morphology could be manipulated using various alcohol/solvent combinations.[13] However, with reactive precipitation the minimum crystal size achieved was ~100 nm, and while electrochemical performance was improved over commercial Li_2S, it was still far short of theoretical capacity. In the case of Li_2S we overcame this issue by eliminating the co-solvent that induced precipitation, allowing the Li_2S produced in Rxn **2** to remain dissolved in ethanol. NCs are recovered by evaporation and purified by a mild annealing treatment. Using this modified solvation/evaporation approach we demonstrated control over NC size (5-25 nm), good uniformity, and cathodes fabricated from these NCs attained theoretical capacity (1164 mAh g^{-1}).[15] Scalable approaches were developed and performance was validated in glassy $70Li_2S$-$30P_2S_5$ electrolytes.[16]

In this work we demonstrate formation of anhydrous Na_2S by either purification of technical grade Na_2S hydrate or via direct synthesis using the liquid-phase reaction between sodium alkoxide and H_2S. Na_2S hydrate is purified by first dehydrating the material using a two-step vacuum annealing process at moderate temperatures followed by high-temperature reduction in hydrogen to remove polysulfide and oxysulfur impurities. Process conditions are identified to produce phase-pure material, and the kinetics of the H_2-reduction process are characterized. Alternatively, we extend the solvation/evaporation route to produce anhydrous Na_2S, demonstrating that methanol is preferred to ethanol as the complexing agent. A complementary suite of characterization techniques (XRD, TGA, FTIR, Raman, and SEM) was employed to

characterize the purity and morphology of Na_2S produced through these processes, which are shown to compare favorably to commercially obtained anhydrous Na_2S. Finally, a basic cost analysis is performed indicating that either route requires materials costs one to two orders of magnitude lower than commercial anhydrous Na_2S.

2. Experimental

2.1. Purification of $Na_2S•xH_2O$.

Sodium sulfide hydrate (Na_2S-h) flakes (60%, Sigma-Aldrich) were ball-milled using a SPEX Mixer/Mill 8000M equipped with ZrO_2 balls for 5 minutes to reduce the particle size. The as-milled material was sieved through a #50 mesh to exclude particles over 300 µm. The milled and sieved Na_2S-h was dehydrated by heating under reduced pressure (~150 mbar) in a vacuum oven. 100 g of Na_2S-h powder was spread in a thin layer (~0.15 g cm^{-2}) on an evaporating tray and placed in the preheated oven at 70 °C and left under vacuum for 12-16 h. The temperature was then increased to 150 °C at a rate of ~1 °C min^{-1} and left for an additional 12-16 h. The furnace was then cooled down at the same rate to 70 °C. Approximately 60 g of dehydrated Na_2S (Na_2S-d) was recovered and placed in an argon filled glove box for further handling and storage.

Impurities were removed from the dehydrated material by reacting with a flowing mixture of 5% H_2 in Ar (General Air, ≥ 99.99%) at elevated temperatures. The reaction was conducted by placing 2 g Na_2S-d in a custom stainless-steel Swagelok reactor (ID = 6.3 mm, length = 70 mm). The reactor was placed in a vertically oriented tube furnace and supplied with 100 sccm of the H_2/Ar mixture. The material was retained in the reactor by use of two stainless-steel Swagelok filter gaskets (pore size = 20 µm) placed at the inlet and exhaust of the reactor. The pressure in the reactor was typically 650 torr (~atmospheric pressure in Golden, CO), and

the composition of the gas effluent was monitored with an on-line quadrupole mass spectrometer (Stanford Research Systems RGA200). The effect of temperature was first investigated by introducing the H_2 gas mixture to a preheated reactor and monitoring the gas effluent for signs of H_2 consumption in the range from 200-500 °C for a time of 2 h. To distinguish the effects of temperature and H_2 reduction, similar experiments were conducted by heating 2 g Na_2S-d under vacuum in a horizontal tube furnace. Once the optimum temperature of 400 °C was established, the kinetics of the H_2 reduction at this temperature were explored by monitoring the time-evolution of the effluent gas composition. In each case, the recovery of H_2-reduced Na_2S (Na_2S-r) from the reactor was over 95% based on the initial mass-loading of Na_2S-d.

2.2. Solution-Based Synthesis of Anhydrous Na_2S.

Sodium sulfide was synthesized using a procedure analogous to that previously reported for Li_2S.[16] First, a sodium alkoxide precursor solution was prepared by reacting sodium metal (1.8 g, Sigma-Aldrich, ACS reagent) with either ethanol (EtOH, Sigma-Aldrich, anhydrous, ≥99.5%) or methanol (MeOH, Sigma-Aldrich, anhydrous, 99.8%) under dry Ar in a glove box in 40 mL quantities with a sodium concentration of 2.0 M. In both cases, the solution was stirred for at least 1 hour to fully dissolve the precursor and allow the solution to equilibrate with room temperature. The precursor solution was then loaded into a 20 mm diameter bubble column reactor (described previously[16]) under Ar, and was reacted with a stoichiometric or near-stoichiometric amount of a 10% H_2S/Ar gas mixture (Matheson) at a rate of 500 sccm (superficial velocity, u = 2.7 cm s^{-1}). The resulting homogeneous product solution (≥ 35 mL) was then retrieved from the bubble column reactor inside a glove box, and aliquoted in 10 mL volumes into an evaporating dish, which was loaded into a horizontal tube furnace and heated to 100 °C under flowing Ar for 2 h. The solid product (~0.88 g, Na_2S-s) was then recovered and

stored under dry Ar in a glove box.

2.3. Materials Characterization.

Commercial samples of technical grade Na_2S from Alfa Aesar were ground in mortar and pestle before characterization to reduce particle size and homogenize the mixture. Thermogravimetric analysis (TGA) was performed by loading approximately 10 mg of sample into an Al_2O_3 pan, which was then transferred into a TGA Q50 (TA Instruments) and heated from 50 to 200 °C at a slow rate of 1.0 °C min^{-1} to prevent melting of hydrate phases. X-ray diffraction (XRD) was measured on a Philips X'Pert X-ray diffractometer with Cu Kα radiation (λ = 0.15405 nm) between 10 and 70° at a scan rate of 5° min^{-1}. Samples were prepared on a glass slide with a piece of Scotch Magic Tape covering the material to prevent undesired reactions with ambient moisture. The contribution from the quartz slide was background subtracted with a polynomial fit. Fourier-transform infrared spectroscopy (FTIR) was performed with a Nicolet Summit FTIR spectrometer using an attenuated total reflection (ATR) accessory equipped with a diamond crystal. Raman spectroscopy was conducted with a WiTec alpha300 M Confocal Microscope/Raman Spectrometer employing a 100 mW 532 nm laser. Samples were mounted on a glass slide and sealed under a quartz cover slip. The laser was focused through the cover slip onto the sample using a 20X objective, and spectra were collected using a CCD detector (Andor Technologies) at -60 °C. Field emission scanning electron microscopy (FESEM) images were taken on a JEOL JSM-7000F FESEM instrument with an accelerating voltage of 5 kV. Particle size was measured with dynamic light scattering (DLS) of a freshly prepared suspension of Na_2S in N-methyl-2-pyrrolidone (NMP) with a ZetaPALS (Brookhaven Instruments).

3. Results & Discussion

3.1. Purification of $Na_2S•xH_2O$.

The as-purchased Na_2S hydrate consists of dense flakes ranging from 0.1-2 cm across with a bright yellow color. The milling and sieving process implemented herein resulted in a homogeneous, free-flowing powder with a pale-yellow color and an average particle size of 28 μm. (Fig. 1-a) TGA of the as-milled hydrate results in approximately 40% mass loss from 50 to 200 °C, which is consistent with the stated composition, and the majority of mass loss occurred below 90 °C with residual mass loss occurring above 100 °C. (Fig. 1-b) FTIR demonstrates a strong absorption band due to O-H stretching at 3,200 cm^{-1} and a moderate peak at 1,570 cm^{-1} due to O-H bending modes, which are attributable to the water of hydration.[17] The strong absorption at 820 cm^{-1} has been attributed to the bending mode of coordinated water.[17] The broad absorption band at 2,800 cm^{-1} corresponds to the S-H stretching mode, indicating the presence of NaHS.[18] FTIR also reveals the presence of other impurities including Na_2SO_x species, such as Na_2SO_4, Na_2SO_3,[19,20] and Na_2SO_2 [20] indicated by the peaks at 1,130 cm^{-1}; 960 and 630 cm^{-1}; and 1,430 cm^{-1}, respectively. (Fig. 1-c) XRD of the milled hydrate results in a complex diffraction pattern reflecting the multitude of hydrate phases including $Na_2S•9H_2O$ (PDF 00-018-1248), $Na_2S•5H_2O$ (PDF 00-018-1249), and $Na_2S•2H_2O$ (PDF 00-040-0521) as well as other unidentified phases. (Fig. 1-d) Finally, Raman spectroscopy shows a doublet peak at Raman shifts of 195 and 240 cm^{-1}. The former has been attributed to the primary Na_2S crystal lattice vibrational mode,[21] while it is speculated that the latter belongs to the same vibrational mode, but has been upshifted due to coordination by water. This explanation is supported by the systematic decrease in relative intensity of the peak at 240 cm^{-1} throughout the dehydration process, which mirrors the attenuation of the FTIR absorbance band at 820 cm^{-1}, which is

attributed to the rocking mode of coordinated water.[17] The Raman spectra also shows a moderate disulfide band at 470 cm^{-1} indicating the presence of Na_2S_x polysulfide species[21] and a water scattering band at 1,700 cm^{-1}.[22] (Fig. 1-e) Detailed peak assignments for FTIR and Raman spectroscopy can be found in Tables S1 and S2, respectively, in the Supporting Information.

When drying hydrated salts, it is crucial to avoid fusing the hydrate, which can lead to decomposition and agglomeration into large particles.[23] The melting point of $Na_2S•xH_2O$ increases with decreasing values of x, e.g. from 49 °C for x = 9 to 98 °C for x = 5.[24] Early accounts of $Na_2S•9H_2O$ dehydration reported drying under vacuum near room temperature in the vicinity of a desiccant for two weeks to achieve the anhydrous product.[25] Later accounts describe the more rapid dehydration of large crystals of the nonahydrate by utilizing a slow (e.g. 2 °C min^{-1}) temperature ramp to avoid melting. However, due to the large size of the crystals, exceedingly high temperatures of 800-900 °C under vacuum were required to achieve full dehydration.[17,19,26] Andersson and Azoulay discovered that the water of hydration could be completely driven off at temperatures as low as 200 °C using nonahydrate crystals with sizes ranging from 0.5-1.0 mm. This later led to the invention of a low temperature, two-step dehydration route by researchers at Sankyo Kasei Co.,[27] which was adapted for this work by heating the milled hydrate under vacuum at 70 °C then 150 °C.

Figure 1 b-e shows the evolution of TGA, FTIR, XRD, and Raman throughout this two-step dehydration. TGA shows a systematic decrease in the volatile content of the material from ~40% in the hydrate to 2% after heating at 70 °C, and finally to the elimination of volatile content after heating at 150 °C. FTIR reflects this systematic decrease in moisture content via attenuation of the signature absorption peaks of the water of crystallization. In addition to

vaporization of water, NaHS apparently undergoes thermal decomposition from 70 – 150 °C as indicated by the attenuation of the strong S-H absorption band at 2,800 cm^{-1}, which is in good agreement with literature reports.[28] It is important to note however that the dehydrated material retains Na_2SO_x impurities. After heating to 70 °C, XRD undergoes a dramatic change from the complex hydrate diffraction pattern to one nearly identical to the expected powder pattern of anhydrous cubic Na_2S (c-Na_2S). However, there is also a signature peak attributed to the orthorhombic phase of Na_2S (o-Na_2S), which has previously been reported to form during the thermal dehydration of the pentahydrate.[19] XRD also detects the presence of some unidentifiable impurity phases not associated with either c-Na_2S or o-Na_2S. In the Raman spectra, the sequential heating steps result in the attenuation of the water scattering band at 1,700 cm^{-1}. The dehydration is also reflected in the simultaneous attenuation of the water-coordinated Na_2S band and growth of the anhydrous Na_2S band. However, polysulfide impurities are retained in the anhydrous material. Color serves as a useful indicator of purity because sodium polysulfides exhibit a range of colors from yellow to gray to red depending on the value of *x* in Na_2S_x[21] while pure Na_2S is pure white. The dehydrated Na_2S maintains a pale-yellow color indicating likely contamination from Na_2S_2 and Na_2S_4.[21] (Fig. 1-a) It has been observed that melting or overheating the material results in various colors, such as brown or red, related to the formation of different polysulfide impurity profiles.

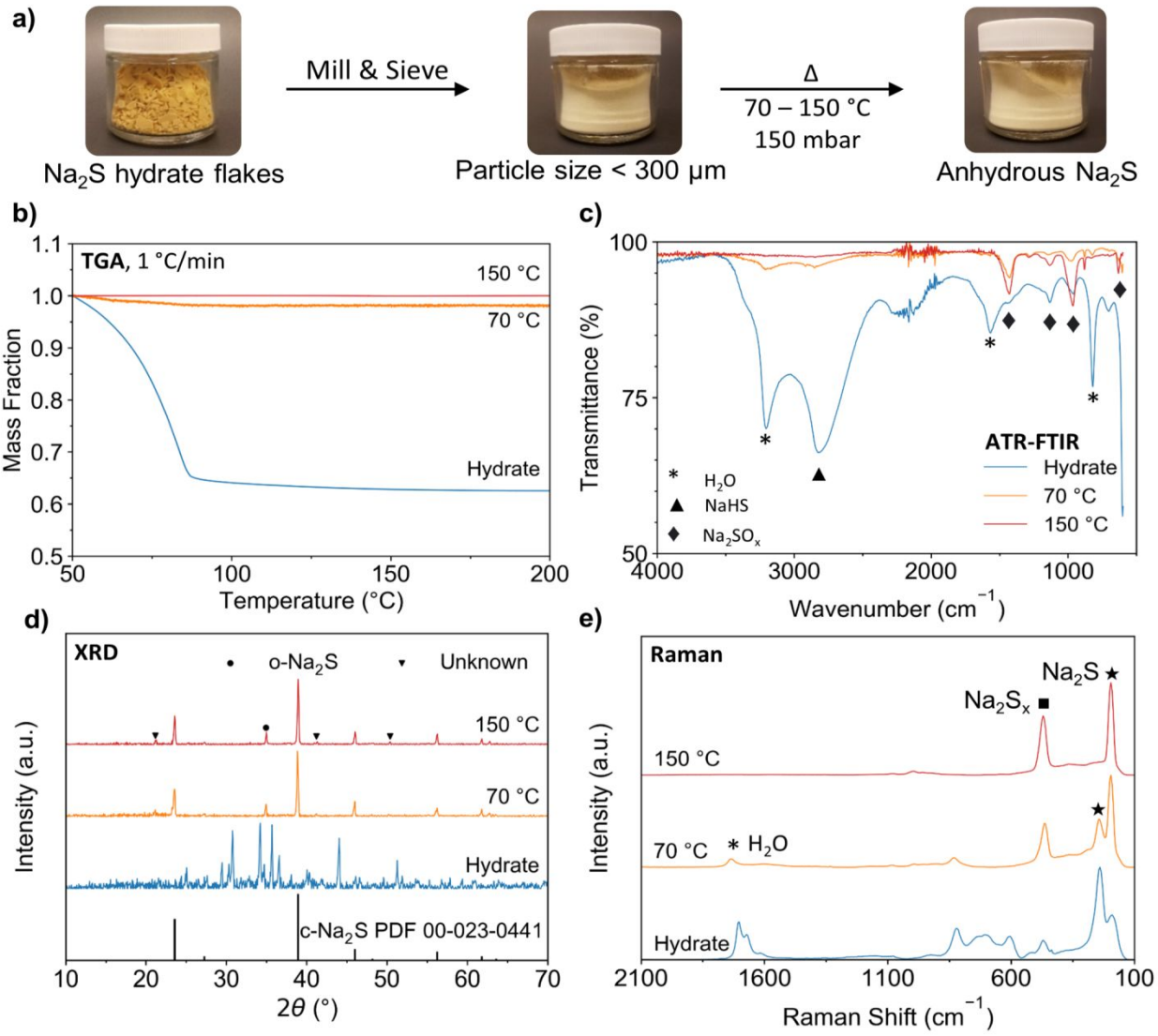

Figure 1. Dehydration of commercial Na_2S hydrate flakes (60%, Sigma-Aldrich). Photograph summary of the dehydration process (a). TGA (b), ATR-FTIR (c), XRD (d), and Raman spectroscopy (e) of milled Na_2S hydrate before treatment, after heating at 70 °C under vacuum, and after subsequently heating at 150 °C under vacuum.

For applications requiring high-purity Na_2S, the dehydrated Na_2S (Na_2S-d) can be reduced under flowing H_2 at elevated temperatures to remove Na_2SO_x and Na_2S_x impurities. In previous studies, this process was conducted at temperatures ranging from 700-900 °C.[19,25] In

this study however, it was found that the process can and should be carried out at much lower temperature. Na_2S-d was reacted under flowing 5% H_2/Ar in a packed-bed reactor at temperatures between 200 and 500 °C, and the H_2 mole fraction in the effluent over time was monitored with on-line mass spectrometry. (Fig. 2-a) At 200 °C no H_2 consumption is detected, and the color of the material is unchanged. However, at 300 °C a small amount of H_2 is consumed as evidenced by a brief decrease in the effluent concentration and a lightening of the material's color. This may be explained by reduction of a surface layer of oxides and polysulfides. At 400 °C, however, there is a sustained decrease in the effluent H_2 concentration indicating ongoing reduction of the material beyond a surface layer, and the material recovered from the reactor exhibits an off-white color. At 500 °C, initially there is significant consumption of H_2, but it could not be sustained due to sintering of the Na_2S powder. In addition, the color of the Na_2S was changed to red indicating further auto-oxidation of the polysulfide species.

Figure 2 b-d compares the evolution of XRD, FTIR, and Raman over increasing temperatures under both 5% H_2/Ar and vacuum to distinguish between the effects of temperature and reaction with H_2. XRD shows that temperature alone has little effect on the crystal structure of the material or its crystalline impurities. Little change is detected for the material treated under H_2 at 200°C, but there is evidence for the formation of crystalline polysulfide species (most likely Na_2S_4),[21] which could indicate reaction between the existing polysulfides and H_2. At 300 °C and above, however, all crystalline impurities are removed to below the detection limit, and there is an apparent rearrangement of the crystal structure from partially orthorhombic to fully cubic. FTIR shows that there is no significant impact of temperature on Na_2SO_x impurities until 500 °C, at which point there is clear decomposition of both forms of impurities. Under flowing H_2 there is a significant reduction in absorbance due to these impurities at 400 °C,

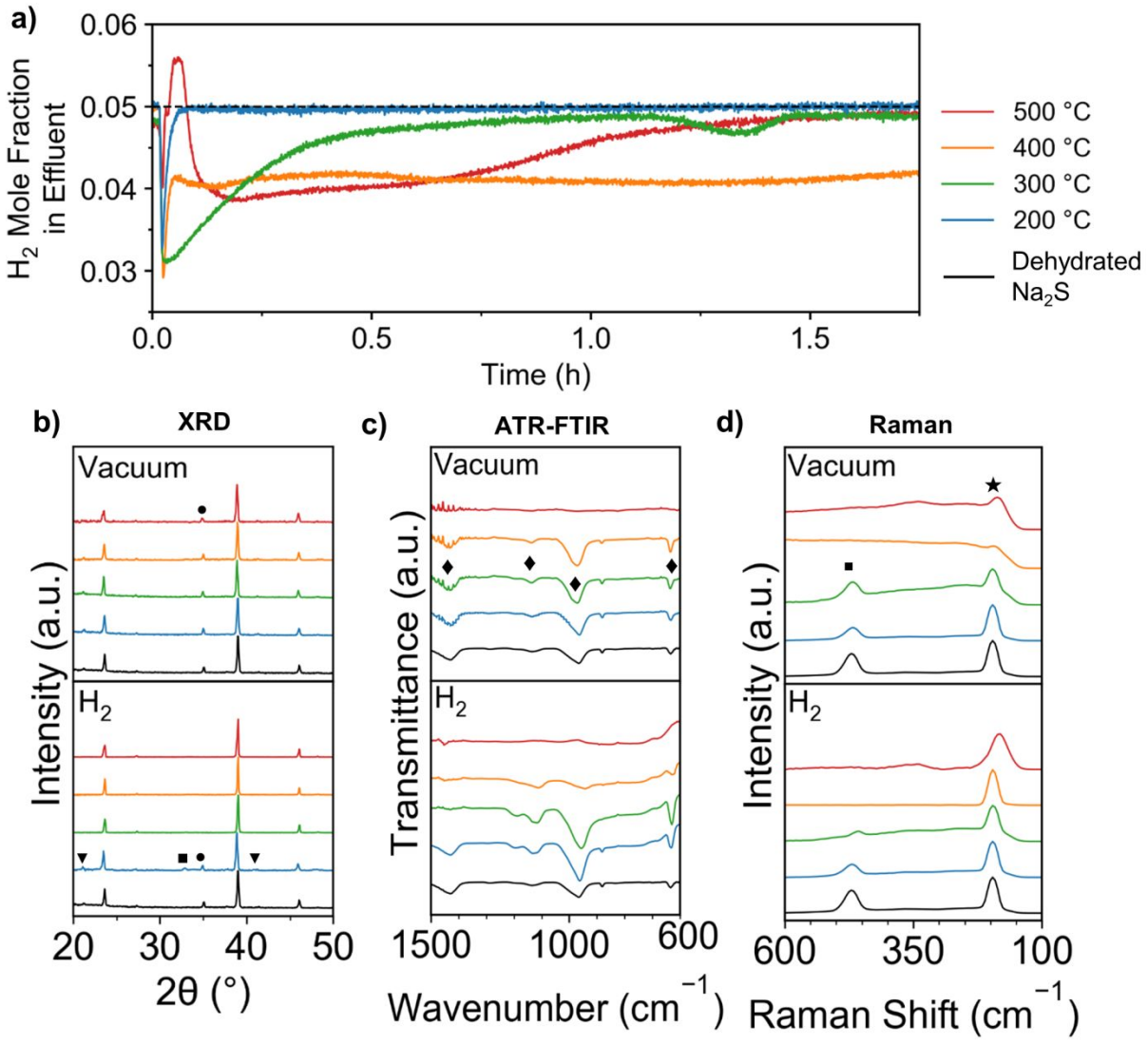

Figure 2. On-line mass spectrometry of gas effluent from a Na_2S-H_2 packed-bed reactor at different bed temperatures. The dashed line at 0.05 represents the mole fraction of H_2 in the inlet gas. (a) Evolution of XRD (b), FTIR (c), and Raman spectroscopy (d) after dehydration (150 ºC) and subsequent heating (200/300/400/500 ºC) under vacuum or H_2/Ar. Key: • - orthorhombic-Na_2S, ▼ – unknown crystalline impurity, ♦ - Na_2SO_x vibrational mode, ■ – Na_2S_x polysulfides, ★ – Na_2S

indicating successful purification at this temperature. In Raman spectroscopy, heating under vacuum alone reduces the intensity of the characteristic Raman shifts of Na_2S and Na_2S_x making

them hard to distinguish from the background, indicating possible melting of the crystalline lattice. Annealing under H_2, however, shows a systematic reduction in the relative amount of polysulfide impurities with increasing temperature up to 400 °C. At 500 ºC the characteristic anhydrous Na_2S Raman signature peak is considerably broadened and shifted, indicating partial decomposition of the desired phase.

The kinetics of the H_2 reduction at 400 °C were explored by ramping the temperature of the reactor to 400 °C and holding for 7 h while monitoring the H_2 mole fraction in the reactor effluent with on-line mass spectrometry. (Fig. 3-a) This data was used to calculate instantaneous rates of H_2 consumption within the reactor, which yields cumulative H_2 consumption upon integration. (Fig. 3-b) The evolution of this cumulative H_2 consumption (or fractional reduction) over time resembles a classic first-order process with no "s-shaped" behavior, indicating that intraparticle mass transfer is the rate-limiting step in the reaction mechanism.[29] A heterogeneous, shrinking-core kinetic model with a pseudo-steady-state approximation as described by Froment et al.[29] was fit to the fractional reduction curve. This model captures the observed behaviour remarkably well, considering it assumes a uniform particle size. A more detailed discussion of the reaction model and fitting procedure is included in the Supporting Information. This model suggests that the required H_2 reduction time could be further reduced by increasing the H_2 partial pressure and/or reducing the particle size. The solid-gas purification route is easily scalable[30] and has been extended to purify 30 g batches of dehydrated Na_2S.

Complementary experiments were performed in which the process was stopped prematurely at specified percent-reduction levels (40 and 80%) to characterize the Na_2S with increasing extent of reaction. As shown in XRD, only a brief anneal under H_2 is required to remove crystalline impurities and for rearrangement into the cubic crystal structure, after which

no change can be detected. (Fig. 3-c) FTIR, however, reveals a more monotonic reduction of Na_2SO_x impurities with increasing extent of reaction. (Fig. 3-d) Finally, Raman spectroscopy indicates a relatively rapid reduction in polysulfide content as evidenced by the near complete attenuation of the disulfide Raman shift at 470 cm^{-1} after only 40% reduction. (Fig. 3-e) This polysulfide removal is reflected in the color of the Na_2S as shown in the insets of Fig. 3-b - the Na_2S undergoes a dramatic color change from pale yellow to an off-white after 40% reduction, and after 100% reduction the Na_2S is nearly pure white.

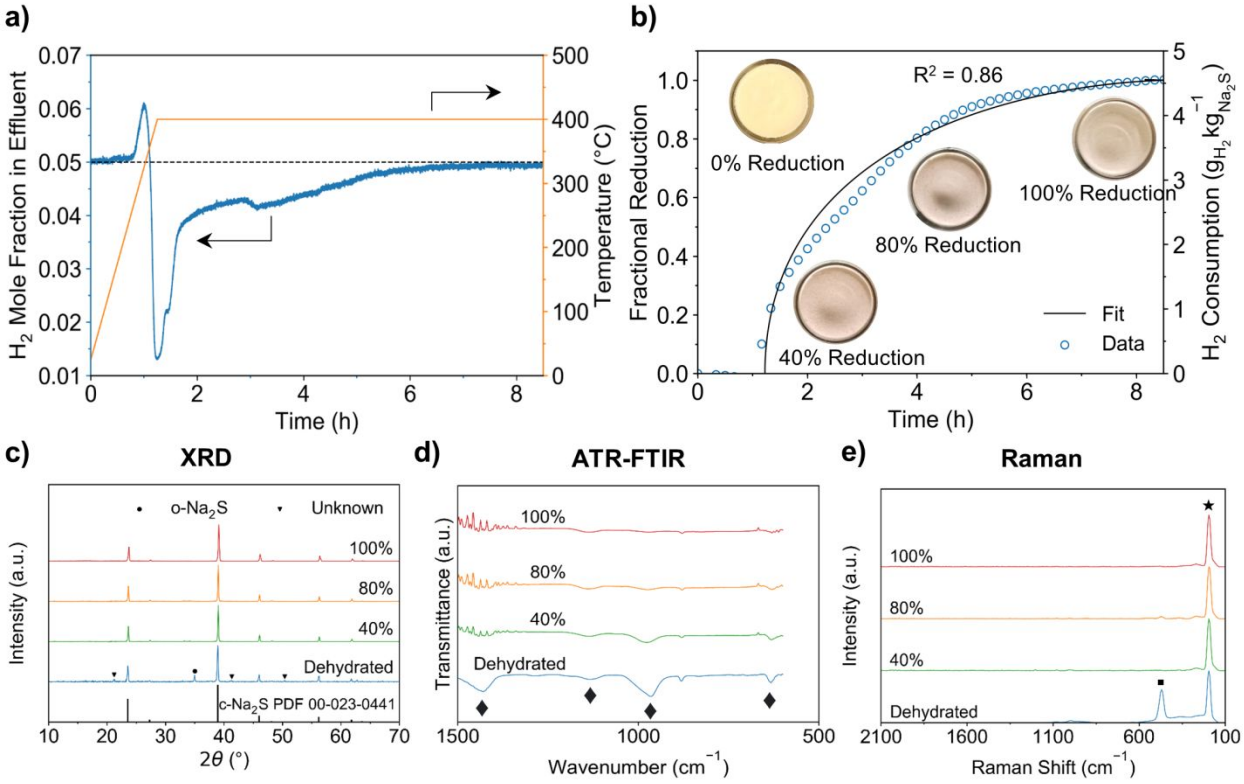

Figure 3. On-line mass spectrometry of gas effluent from a Na_2S-H_2 packed-bed reactor over time with the corresponding bed temperature (a); cumulative H_2 consumption in the same reactor as a function of time with core-shell model fit and photographs of Na_2S at varying degrees of reduction (b); XRD (c), FTIR (d), and Raman spectroscopy (e) of Na_2S at varying degrees of reduction. Key: • - orthorhombic-Na_2S, ▼ – unknown crystalline impurity, ♦ - Na_2SO_x vibrational mode, ■ – Na_2S_x polysulfides, ★ – Na_2S

3.2. Solution-Based Synthesis of Anhydrous Na_2S.

The solution-based synthesis in ethanol was found to be very sensitive to the stoichiometry of H_2S/NaOEt. XRD data for synthesized Na_2S in EtOH with different H_2S amounts are shown in Fig. 4 a-c. When an exact stoichiometric ratio of H_2S/NaOEt was supplied to the reactor, a NaHS impurity was detected in the recovered Na_2S, possibly due to a small amount of solution loss when transferring the solution into the bubble column. When 92% of the stoichiometric amount of H_2S was used, unreacted NaOEt was detected in the recovered Na_2S. At 95% of the stoichiometric amount of H_2S there was no NaOEt or NaHS detected in the final Na_2S. In addition, sub-stoichiometric amounts of H_2S also lead to a preferential orientation in the recovered crystals that was distinct from the Na_2S XRD powder pattern. When methanol was used as the solvent for the solution-based synthesis the sensitivity to changes in stoichiometry were not present. Using methanol, the delivery of a stoichiometric amount of H_2S to the reactor resulted in the expected Na_2S powder pattern with no impurities present and a significantly reduced background. (Fig. 4-d)

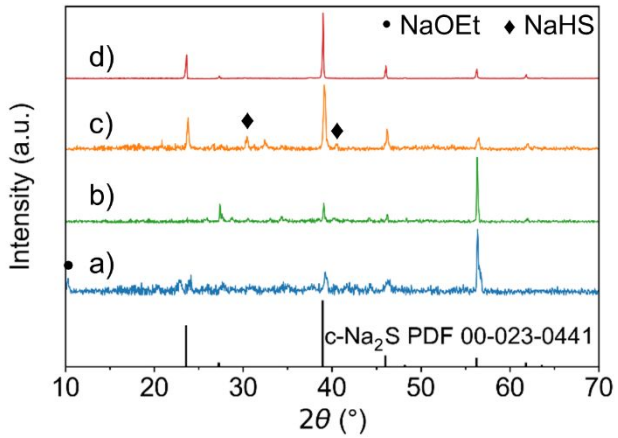

Figure 4. XRD of synthesized Na_2S recovered from ethanol by drying at 100 °C (a-c) after reaction with 92, 95, and 100% of the stoichiometric amount of H_2S, respectively, and of

synthesized Na_2S recovered from methanol by drying at 100 °C after reaction with 100% of the stoichiometric amount of H_2S (d).

3.3. Comparison with Commercial Anhydrous Na_2S.

Anhydrous Na_2S produced from dehydration and H_2 reduction of technical grade hydrate as well as the methanol-based synthesis were compared directly to commercial anhydrous Na_2S purchased from both Sigma-Aldrich and Alfa Aesar using TGA, FTIR, XRD, and Raman spectroscopy. (Fig. 5) In almost all samples, TGA revealed little or no mass loss up to 200 °C, indicating the very low moisture content of all materials. The material sourced from Alfa Aesar exhibits a mass loss of ~1.5 wt%, and the synthesized Na_2S loses a small (~0.5 wt%) amount of mass below 70 °C. The mass loss experienced by the synthesized material is attributed to evaporation of a surface layer of moisture that is adsorbed while loading the sample into the Ar-blanketed furnace for TGA. Drying the synthesized Na_2S at yet higher temperatures results in a similar mass loss in TGA, and no signature alcohol peaks are present in FTIR or Raman, so it is concluded this minor mass loss is due to adsorbed moisture rather than retained solvent from the synthesis.

The dehydrated material retained significant impurities including the presence of the orthorhombic phase in XRD, Na_2SO_x species in FTIR, and polysulfides in Raman. Both commercial samples of Na_2S were phase-pure with respect to XRD but retained typical Na_2SO_x impurities, albeit in much lower concentrations than the dehydrated material. However, FTIR shows the presence of residual H_2O content in the Sigma Aldrich Na_2S and Raman shows that it contains appreciable polysulfide impurities, consistent with its pale-yellow color. The Alfa Aesar material, on the other hand, possessed nearly undetectable levels of polysulfide species in

Raman, but a significant amount of Na_2SO_4 as indicated by the strong IR absorption in the SO_4^{2-} symmetric stretching region. Nagy et al. characterized the polysulfide content of commercial sodium sulfide in different grades by absorbance measurements of 150 mM solutions in distilled water.[31] They found similar polysulfide levels of (0.1 – 0.6%) for both the anhydrous and hydrate forms. In contrast to this work, they found higher levels of polysulfide in the Alfa Aesar relative to Sigma. Such variation may reflect batch to batch variability, highlighting the importance of the characterization methods described herein for applications where the impurity profile is a concern.

Hydrogen reduction at 400ºC and the solution synthesized Na_2S displayed the highest purity. Both were phase–pure with respect to XRD and there was no evidence of the polysulfide band in their Raman spectra. FTIR proved to be the most sensitive diagnostic. Both forms were free of impurities with the exception of low intensity absorption signatures from oysulfur groups, and arguably the solution synthesized Na_2S was superior to the H_2-reduced.

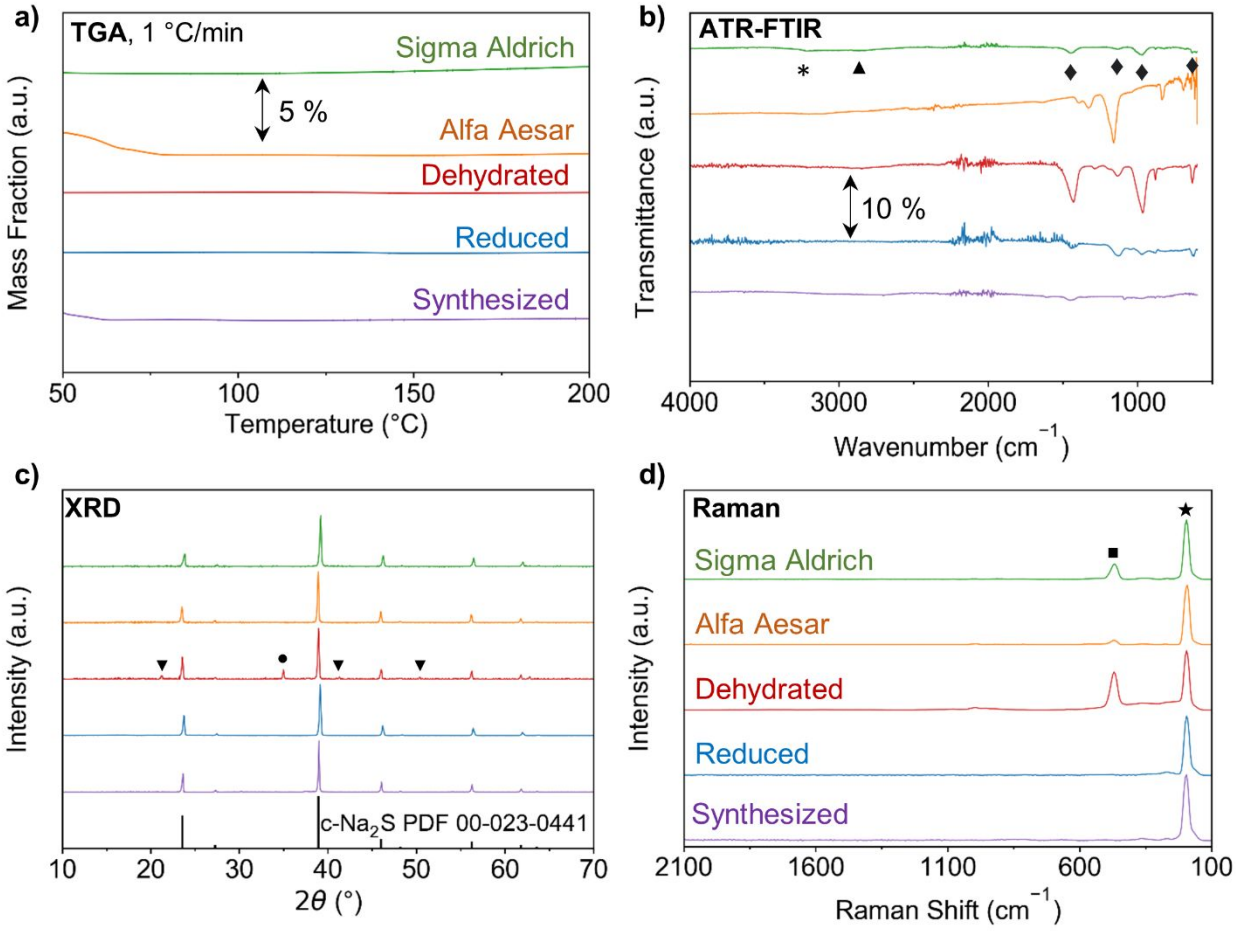

Figure 5. Comparison using TGA (a), FTIR (b), XRD (c), and Raman spectroscopy (d) of the anhydrous Na_2S produced in this work. Key: * - H_2O, ♦ - S=O vibrational mode, ▲ – NaHS, ▼ – unknown crystalline impurity, • - o-Na_2S, ■ – Na_2S_x, ★ – Na_2S

The variation in microstructure among the different Na_2S samples was characterized using SEM (Fig. 6) along with their respective photographs to provide context of color and macroscopic texture. Commercial and dehydrated Na_2S displayed similar morphologies consisting of polydisperse nodules with little surface roughness or micro-features. However, the dehydrated Na_2S undergoes a dramatic structural rearrangement during hydrogen reduction. The smaller particles from the dehydrated material appear to coalesce during reduction to form somewhat larger, more uniform particles with a highly porous skeletal structure. In contrast to the other forms, the solution-synthesized Na_2S possesses a very fine microstructure with small, monodisperse particles on the order of 1-10 μm in diameter. Both the skeletal structure and the uniformly small particle size of reduced and synthesized Na_2S, respectively, could have important impacts on reactivity owing to their higher specific surface area. The small particle size, monodisperse nature, and high purity of Na_2S-s could make it especially relevant to emerging applications in energy storage, such as high-capacity Na-S cathode materials or as a precursor to Na_2S-based solid-state electrolytes, the synthesis of which would presumably benefit from smaller particle size and higher surface area of the Na_2S reagent. Lower magnification images, and images of the as-milled Na_2S-h are provided in the Supporting Information.

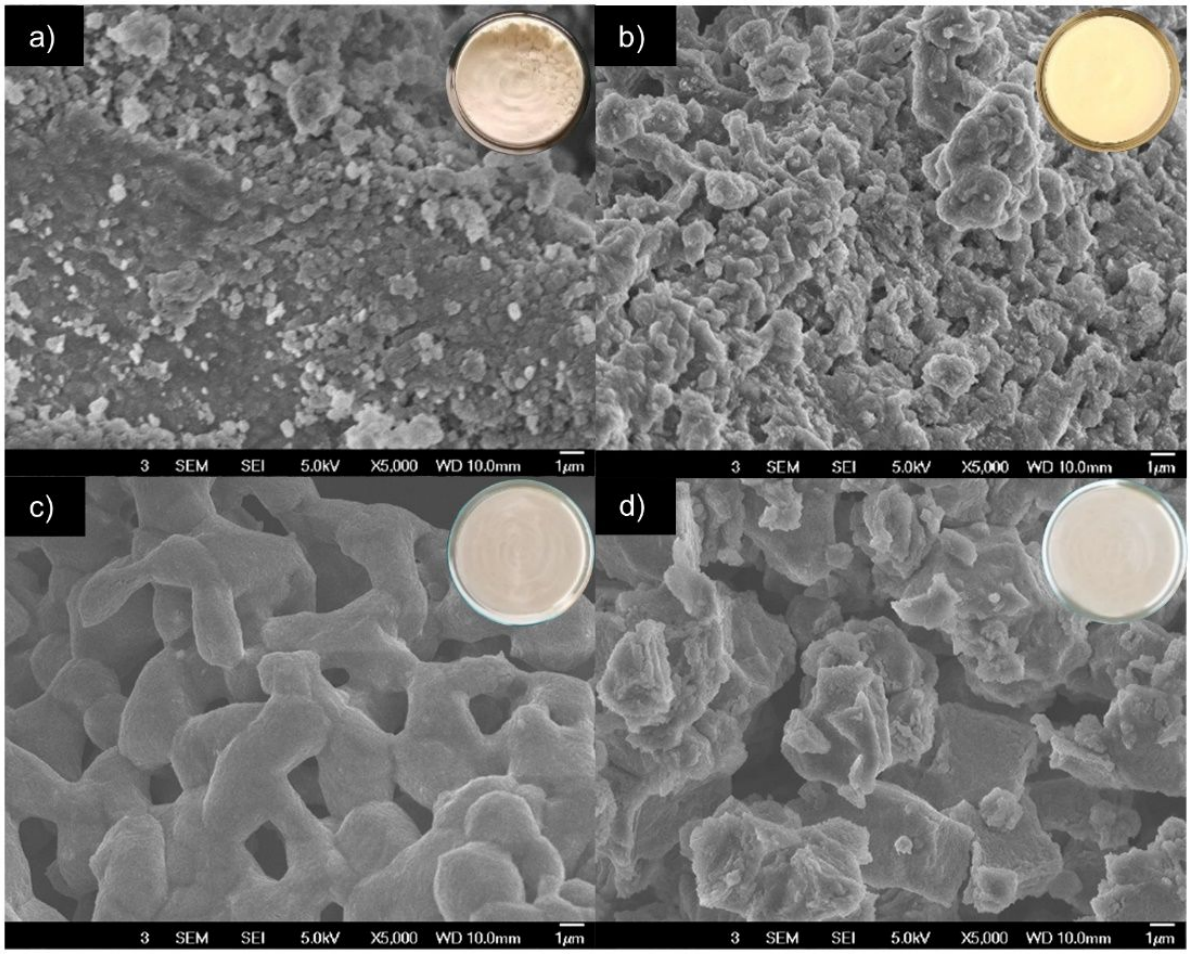

Figure 6. SEM of Na_2S from different preparation routes and corresponding photograph (inset): commercial anhydrous from Sigma Aldrich (a); dehydrated (b); H_2-reduced (c); and synthesized (methanol system) (d).

Finally, the potential material cost of the described methods of Na_2S preparation and purification are compared to the current cost of anhydrous Na_2S. Though pricing of research-grade materials is not always directly relevant to prices at bulk scales, in this case the low availability of anhydrous Na_2S in bulk quantities necessitates their use. Table S3 provides a summary of reagent costs. Solid reagent pricing was retrieved from the Sigma-Aldrich website for reagent-grade chemicals (accessed October 2020), while gaseous

reagent prices are typical for industrial use. The cost to produce Na_2S is not expected to be very sensitive to the cost of gaseous reagents due to their much lower molar price, which are at least two orders of magnitude lower than the solid reagents. The reagent costs per gram-Na_2S for Na_2S-d, Na_2S-r, and Na_2S-s are derived from the stated reagent costs and then shown in comparison to two commercial forms of anhydrous Na_2S – Sigma Aldrich and Alfa Aesar – in Fig. 7, revealing that dehydration and purification of Na_2S-h and the liquid-phase synthesis route could be one and two orders of magnitude cheaper than the current commercially available material, respectively. The difference is driven by the cost of sodium source, with metallic sodium being considerably more expensive than the technical grade hydrate. Table S3 shows pricing of research grade materials. Both technical grade Na_2S hydrate and Na metal are widely available commodity chemicals at pricing two orders of magnitude below the values shown in Table S3, suggesting that at scale anhydrous Na_2S produced through either method would be a very low cost. Finally, Table 1 provides a summary of the different samples of Na_2S investigated in this work.

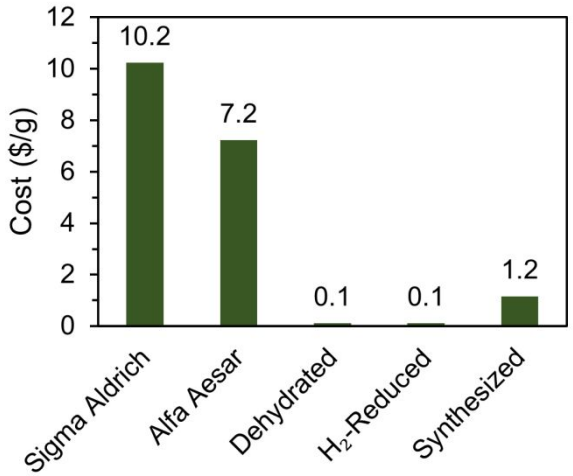

Figure 7. Materials cost comparison of different Na_2S grades at lab-scale.

Table 1. Summary of Na_2S samples investigated in this work.

Source	Form/Color	TGA Mass Loss (wt%)	XRD Crystalline Phases	FTIR Impurities	Raman Impurities	Materials Cost Estimate ($ g^{-1}-Na_2S)
Sigma Aldrich (97-103%)	Granular/Powder Pale Yellow	ND*	c-Na_2S	H_2O (trace) NaHS (trace) Na_2SO_4 (trace) Na_2SO_3 (trace) Na_2SO_2 (trace)	Na_2S_x	10.2
Alfa Aesar (>95%)	Large Chunks Yellow surface coating, off-white interior	1.5	c-Na_2S	Na_2SO_4 Na_2SO_3 (trace)	Na_2S_x (trace)	7.2
$Na_2S•xH_2O$ Sigma (>60% Na_2S)	Large Flakes Yellow-Orange	38.5	$Na_2S•9H_2O$ $Na_2S•5H_2O$ $Na_2S•2H_2O$ Various unidentified	H_2O NaHS Na_2SO_4 Na_2SO_3 Na_2SO_2	Na_2S_x H_2O	0.1
Dehydrated $Na_2S•xH_{2O}$	Powder Yellow	ND	c-Na_2S o-Na_2S Trace Unidentified	H_2O (trace) NaHS (trace) Na_2SO_4 (trace) Na_2SO_3 Na_2SO_2	Na_2S_x	0.1
H_2-Reduced	Powder Pure white	ND	c-Na_2S	Na_2SO_4 (trace) Na_2SO_3 (trace) Na_2SO_2 (trace)	ND	0.1

Synthesized (MeOH)	Fine Powder Pure white	0.5	c-Na_2S	Na_2SO_2 (trace)	ND	1.2

***ND = Not Detected**

4. Conclusions

Two methods to prepare anhydrous Na_2S of high purity have been described in this work. First, low-cost Na_2S hydrate was dehydrated and then purified under flowing H_2. It was found that optimal reduction occurred at T = 400 ºC, significantly lower than previous reports, through a diffusion limited process that was well described by a shrinking core model. The reduction process produced a unique skeletal microstructure. Second, Na_2S was formed via reaction of H_2S gas with a dissolved sodium alkoxide and recovered by solvent evaporation at moderate temperatures with no further purification. Methanol robustly produced phase-pure Na_2S with a narrow particle size distribution, whereas in ethanol minor stoichiometry variations resulted in impurity phases.

The purity of material produced from both routes were compared to two commercial forms of Na_2S anhydride. All four materials were indistinguishable by XRD, but vibrational spectroscopies proved to be more sensitive diagnostics. Commercial Na_2S contained appreciable polysulfide (Raman) and Na_2SO_x (FTIR) impurities. Polysulfide signatures were eliminated and Na_2SO_x signals greatly attenuated in both synthesis methods presented, with the solution-based synthesis perhaps being slightly superior. Color is a sensitive and cost-effective diagnostic, with pure white being the hallmark of phase pure, impurity free Na_2S. Both solution synthesis and the hydrate reduction processes are readily

scalable with materials costs one and two orders of magnitude lower than the price of commercially available Na_2S, respectively.

Acknowledgements

This work was supported by the US National Science Foundation through Award 1825470.

Supporting Information

Spectroscopic peak assignments, additional SEM images – including lower magnifications and milled Na_2S hydrate – lab-scale reagent cost summary, and shrinking-core reaction model details.

References

1. Xu X, Zhou D, Qin X, et al. A room-temperature sodium–sulfur battery with high capacity and stable cycling performance. Nat Commun. 2018;9(1).
2. Yang H, Zhang B, Wang YX, et al. Alkali-Metal Sulfide as Cathodes toward Safe and High-Capacity Metal (M = Li, Na, K) Sulfur Batteries. Advanced Energy Materials. 2020;10(37):2001764.
3. Yu X, Manthiram A. Performance Enhancement and Mechanistic Studies of Room-Temperature Sodium–Sulfur Batteries with a Carbon-Coated Functional Nafion Separator and a Na2S/Activated Carbon Nanofiber Cathode. Chemistry of Materials. 2016;28(3):896-905.
4. Noi K, Hayashi A, Tatsumisago M. Structure and properties of the Na2S–P2S5 glasses and glass–ceramics prepared by mechanical milling. Journal of Power Sources. 2014;269:260-265.
5. Hayashi A, Masuzawa N, Yubuchi S, et al. A sodium-ion sulfide solid electrolyte with unprecedented conductivity at room temperature. Nat Commun. 2019;10(1).
6. Dive A, Zhang Y, Yao Y, et al. Investigations of the structure of Na2S + P2S5 glassy electrolytes and its impact on Na+ ionic conductivity through ab initio molecular dynamics. Solid State Ionics. 2019;338:177-184.
7. Miura A, Ito H, Bartel C, et al. Selective metathesis synthesis of MgCr2S4 by control of thermodynamic driving forces [10.1039/C9MH01999E]. Materials Horizons. 2020.
8. Chandrasekaran S, Yao L, Deng L, et al. Recent advances in metal sulfides: from controlled fabrication to electrocatalytic, photocatalytic and photoelectrochemical

water splitting and beyond. Chemical Society Reviews. 2019 Jul 29;48(15):4178-4280.
9. Zhang F, Wong SS. Controlled Synthesis of Semiconducting Metal Sulfide Nanowires. Chemistry of Materials. 2009;21(19):4541-4554.
10. Borodkin Y, Rusanov E, Marchenko A, et al. Synthesis and chemical properties of Di(2-fluoro-2-polyfluoroalkyl- alkenyl)sulfides and 2,6-bis(polyfluoroalkyl)-1,4-oxathiine 4,4-dioxides. Journal of Sulfur Chemistry. 2019;40(4):416-425.
11. Szabo C, Papapetropoulos A. International Union of Basic and Clinical Pharmacology. CII: Pharmacological Modulation of H2S Levels: H2S Donors and H2S Biosynthesis Inhibitors. Pharmacological Reviews. 2017 Oct;69(4):497-564.
12. Butts D, Bush DR. Sodium Sulfates and Sulfides. Kirk-Othmer Encyclopedia of Chemical Technology. New York: John Wiley & Sons, Inc; 2013.
13. Li X, Zhao Y, Brennan A, et al. Reactive Precipitation of Anhydrous Alkali Sulfide Nanocrystals with Concomitant Abatement of Hydrogen Sulfide and Cogeneration of Hydrogen. ChemSusChem. 2017 Jul 21;10(14):2904-2913.
14. Hietala K, Zhao Y, Yang Y, et al. Scalable Synthesis of Alkali Sulfide Nanocrystals Using a Bubble Column Reactor. Industrial & Engineering Chemistry Research. 2018;57(25):8436-8442.
15. Zhao Y, Yang Y, Wolden CA. Scalable Synthesis of Size-Controlled Li2S Nanocrystals for Next-Generation Battery Technologies. ACS Applied Energy Materials. 2019;2(3):2246-2254.
16. Zhao Y, Smith W, Wolden CA. Scalable synthesis of Li2S nanocrystals for solid-state electrolyte applications. Journal of the Electrochemical Society. 2020;167.
17. Kizilyalli M, Bilgin M, Kizilyalli HM. Solid-state synthesis and X-ray diffraction studies of Na2S. Journal of Solid State Chemistry. 1990;85(2):283-292.
18. Beckenkamp K, Lutz HD, Jacobs H, et al. Polymorphism and Phase Transitions of the Isostructural MSH (M = Na, K, and Rb). Journal of Solid State Chemistry. 1994;109(2):241-250.
19. Rosen E, Tegman R. A preparative and X-ray powder diffraction study of the polysulfides Na2S2, Na2S4 and Na2S5. Acta Chemica Scandinavica. 1971;25:3329-3336.
20. Nakamoto K. Infrared and Raman Spectra of Inorganic and Coordination Compounds. Handbook of Vibrational Spectroscopy: John Wiley & Sons, Ltd.; 2006.
21. Zhang Q. The synthesis and characterization of sodium polysulfides for Na-S battery application: Virginia Polytechnic Institute and State University; 2019.
22. Cross PC, Burnham J, Leighton PA. The Raman Spectrum and the Structure of Water. Journal of the American Chemical Society. 1937;59(6):1134-1147.
23. Barstow EO, Heath SB, inventors; Dow Chemical Co, assignee. Process of Dehydrating Magnesium Chloride patent US1874735. 1929.
24. Anderson JY, Azoulay M. Mechanism and kinetics of the thermal decomposition of sodium sulphide pentahydrate under controlled water vapour pressure. J Chem Soc, Dalton Trans. 1986:469-475.
25. Courtois MG, Lebeau MP. Preparation of Anhydrous Sodium Sulfide. Weekly reports of meetings of the Académie des sciences. 1938 (207):1220-1221.

26. Copes JP, McKinley C, inventors; General Aniline & Film Corporation, assignee. Dehydration of Sodium Sulfide. U.S.A. patent US2533163. 1950.
27. Maeda K, Aoyama Y, inventors; Sankyo Kasei Co., assignee. Process for preparing crystals of anhydrous sodium sulfide patent US5071632. 1991.
28. Sheppard DA, Jepsen LH, Jensen TR, et al. New directions for hydrogen storage: sulphur destabilised sodium aluminium hydride. Journal of Materials Chemistry A. 2013;1(41):12775.
29. Froment GF, Bischoff KB, De Wilde J. Heterogeneous Model with Shrinking Unreacted Core. Chemical reactor analysis and design. Hoboken, NJ: John Wiley & Sons, Inc; 2011.
30. Cho H, Walker S, Plunkett M, et al. Scalable Gas-Phase Purification of Boron Nitride Nanotubes by Selective Chlorine Etching. Chemistry of Materials. 2020;32(9):3911-3921.
31. Nagy P, Palinkas Z, Nagy A, et al. Chemical aspects of hydrogen sulfide measurements in physiological samples. Biochim Biophys Acta. 2014 Feb;1840(2):876-91.

Supporting Information - Production and Purification of Anhydrous Sodium Sulfide

William H. Smith, Jerry Birnbaum, and Colin A. Wolden*

Department of Chemical and Biological Engineering
Colorado School of Mines, Golden, CO, USA
*Email: cwolden@mines.edu

Table S1. FTIR Peak Assignments

Wavenumber (cm^{-1})	Vibrational Mode	Chemical Identity	References
3,200	H_2O Stretch	H_2O	[1]
2,800	H-S Stretch	NaHS	[2]
1,570	H_2O Bending	H_2O	[1]
1,430	SO_2^{2-} Asymmetric Stretch	Na_2SO_2	[3]
1,130	SO_4^{2-} Symmetric Stretch	Na_2SO_4	[3]
960	SO_3^{2-} Symmetric Stretch	Na_2SO_3	[3]
820	Coordinated H_2O Bending	H_2O	[1]
630	SO_3^{2-} Bending	Na_2SO_3	[3]

Table S2. Raman Peak Assignments

Raman Shift (cm^{-1})	Vibrational Mode	Chemical Identity	References
1,700	H_2O Bending	H_2O	[1]
470	S_2^{2-}/S_4^{2-} Stretch	Na_2S_2/Na_2S_4	[4]
240	Water Coordinated Na_2S Lattice Vibration	Na_2S	
195	Na_2S Lattice Vibration	Na_2S	[4]

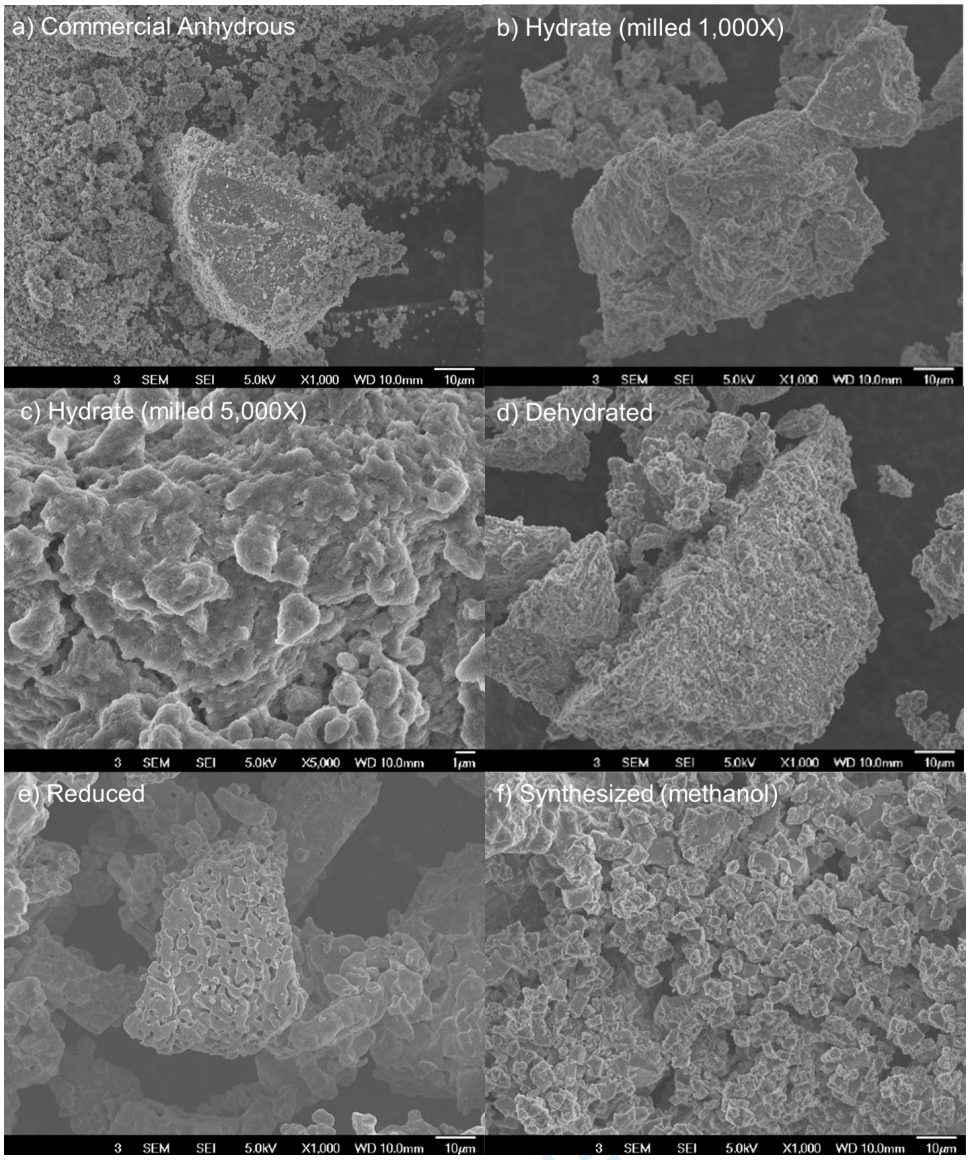

Fig. S1. Lower magnification SEM images of Na_2S from different preparation routes: commercial anhydrous (a), as-milled hydrate at 1,000X (b) and 5,000X (c) magnifications, dehydrated (d), H_2-reduced (e), and synthesized (methanol system) (f).

Table S3. Prices of Na_2S reagents

Chemical	Quantity (g)	Price ($)	Unit Price ($ g^{-1})	Molar Mass (g mol^{-1})	Unit Price ($ mol^{-1})
Na_2S Anhydride (Sigma Aldrich)	50	512.00	10.24	78.04	799.13
Na_2S Anhydride (Alfa Aesar)	100	723.00	7.23	78.04	564.23
Na_2S Hydrate (60%)[a]	1000	66.00	0.07	54.02	3.57
H_2[b]	1000	3.50	0.00	2.02	0.01
Na Metal[a]	50	$98.30	1.97	22.99	45.20
H_2S[b]	1000	$2.00	0.00	34.10	0.07

[a]Sigma-Aldrich pricing

[b]Estimates

Shrinking-Core Reaction-Model Details

The chemical basis of the hydrogen-reduction purification process is the reaction of H_2 gas with oxidized impurities in the anhydrous Na_2S including polysulfides (Na_2S_x) and oxysulfur compounds (Na_2SO_x). The chemical reactions underlying this process are:

$$H_2(g) + Na_2S_x(s) \rightarrow Na_2S(s) + H_2S_{x-1}(g); \quad x > 1 \#(\text{Rxn. } 1)$$

$$(x-1)H_2(g) + Na_2S_x(s) \rightarrow Na_2S(s) + (x-1)H_2S(g); \quad x > 1 \#(\text{Rxn. } 2)$$

$$xH_2(g) + Na_2SO_x(s) \rightarrow Na_2S(s) + xH_2O(g); \quad 2 \leq x \leq 4 \#(\text{Rxn. } 3)$$

The kinetics of the hydrogen-reduction reaction at 400 °C were modeled using a single heterogeneous gas-solid reaction controlled by gas diffusion through a shrinking unreacted core with a pseudo-steady-state approximation, assuming a uniform particle size of 28 μm. The external film mass transfer and gas-solid reaction are assumed to be much faster than internal gas diffusion – an assumption that is well-supported by the first-order nature of the fractional reduction curve: A lack of s-shaped behavior is characteristic of a large Thiele Modulus ($\phi'' = R_p\sqrt{\frac{k\rho_s}{D_{e,A}}}$ for zero-order gas-solid reaction kinetics in a spherical particle) indicating the process is internal-diffusion-limited.

For an internal-diffusion-limited gas-solid reaction, the time, t, required to achieve fractional conversion, x, is given by the following relations:[5]

$$t = \frac{R_p^2\, aC_{s0}}{C_{H_2} D_{e,H_2}}\left(\frac{1}{2}\left[1-\left(\frac{r_c}{R_p}\right)^2\right] - \frac{1}{3}\left[1-\left(\frac{r_c}{R_p}\right)^3\right]\right) \#(1)$$

$$x = \frac{\int_0^t \dot{n}_{H_2} dt}{\int_0^\infty \dot{n}_{H_2} dt} = 1 - \left(\frac{r_c}{R_p}\right)^3 \#(2)$$

The experimental H_2 flowrate vs. time data (Fig. 3a) was used to calculate fractional conversion vs. time (Fig. 3b), which was fit to the above model using the method of least squares. The domain was limited to time larger than 1.22 h to avoid the impact of flow instabilities at the beginning of the reaction, which manifest as an apparent increase of H_2 flow in the effluent. This instability is possibly caused by partial sintering of the reactant bed leading to a temporary change in pressure at the inlet of the mass spectrometer. The apparent increase in H_2 concentration is explained by the slower pumping speed of H_2 relative to Ar during this pressure fluctuation. Because it is difficult and time-consuming to extract values for a, C_{s0}, and D_{e,H_2}, these values were instead lumped into a single fit parameter, B with a best-fit value of $B = \frac{aC_{s0}}{D_{e,H_2}} = 5.75 \cdot 10^{14} \frac{\text{mol } H_2 \cdot \text{s}}{\text{m}_{\text{solid}}^3 m^2}$.

The coefficient of determination, R^2, was calculated according to the following equations, and the best fit value was found to be $R^2 = 0.86$.

$$R^2 = 1 - \frac{SS_{res}}{SS_{tot}} \#(3)$$

$$SS_{res} = \sum_i (y_i - f_i)^2 \#(4)$$

$$S_{res} = \sum_i (y_i - \bar{y})^2 \#(5)$$

List of Symbols

Letters		*Units*
a	Number of moles of H_2 reacting with 1 mole of solid reactant	$\frac{\text{mol } H_2}{\text{mol S}}$
B	Lumped fit parameter $= \frac{aC_{s0}}{D_{e,H_2}}$	$\frac{\text{mol } H_2 \cdot \text{s}}{\text{m}_{\text{solid}}^3 \text{m}^2}$
C_{H_2}	Concentration of H_2 in gas phase	$\frac{\text{mol } H_2}{\text{m}^3}$
C_{s0}	Initial concentration of the solid reactant	$\frac{\text{mol S}}{\text{m}^3}$
D_{e,H_2}	Effective diffusivity of H_2 in the solid	$\frac{\text{m}^2}{\text{s}}$
f_i	Fitted/Model-predicted value	
k	Reaction rate constant	$\frac{\text{mol } H_2}{\text{kg}_{\text{solid}} \cdot \text{s}}$
$\dot{n}_{H_2}$	Molar rate of H_2 consumption	$\frac{\text{mol } H_2}{\text{s}}$
R^2	Coefficient of determination	
r_c	Radius of unreacted core	m
R_p	Particle radius	m
S	Solid reactant	
SS_{res}	Sum of squares of residuals	
SS_{tot}	Total sum of squares	
t	Reaction time	s
x	Fractional conversion/reduction	
$\bar{y}$	Mean value of observed data	
y_i	Value of observed data	

Greek Symbols		*Units*
ρ_s	Skeletal solid mass density	$\frac{\text{kg}}{\text{m}_{\text{solid}}^3}$
ϕ''	Thiele Modulus for zero-order gas-solid reaction kinetics in a spherical particle	

References

1. Kizilyalli M, Bilgin M, Kizilyalli HM. Solid-state synthesis and X-ray diffraction studies of Na2S. J Solid State Chem. 1990;85(2):283-292.
2. Beckenkamp K, Lutz HD, Jacobs H, et al. Polymorphism and Phase Transitions of the Isostructural MSH (M = Na, K, and Rb). J Solid State Chem. 1994;109(2):241-250.
3. Nakamoto K. Infrared and Raman Spectra of Inorganic and Coordination Compounds. Handbook of Vibrational Spectroscopy: John Wiley & Sons, Ltd.; 2006.

4. Zhang Q. The synthesis and characterization of sodium polysulfides for Na-S battery application: Virginia Polytechnic Institute and State University; 2019.
5. Froment GF, Bischoff KB, De Wilde J. Heterogeneous Model with Shrinking Unreacted Core. Chemical reactor analysis and design. Hoboken, NJ: John Wiley & Sons, Inc; 2011.